A primary culture system of mouse thick ascending limb cells with preserved function and uromodulin processing

Glaudemans, Bob ; Terryn, Sara ; Gölz, Nadine ; Brunati, Martina ; Cattaneo, Angela ; Bachi, Angela ; Al-Qusairi, Lama ; Ziegler, Urs ; Staub, Olivier ; Rampoldi, Luca ; Devuyst, Olivier

Abstract: The epithelial cells lining the thick ascending limb (TAL) of the loop of Henle perform essential transport processes and secrete uromodulin, the most abundant protein in normal urine. The lack of differentiated cell culture systems has hampered studies of TAL functions. Here, we report a method to generate differentiated primary cultures of TAL cells, developed from microdissected tubules obtained in mouse kidneys. The TAL tubules cultured on permeable filters formed polarized confluent monolayers in 12 days. The TAL cells remain differentiated and express functional markers such as uromodulin, NKCC2, and ROMK at the apical membrane. Electrophysiological measurements on primary TAL monolayers showed a lumen-positive transepithelial potential ($+9.4 \pm 0.8$ mV/cm(2)) and transepithelial resistance similar to that recorded in vivo. The transepithelial potential is abolished by apical bumetanide and in primary cultures obtained from ROMK knockout mice. The processing, maturation and apical secretion of uromodulin by primary TAL cells is identical to that observed in vivo. The primary TAL cells respond appropriately to hypoxia, hypertonicity, and stimulation by desmopressin, and they can be transfected. The establishment of this primary culture system will allow the investigation of TAL cells obtained from genetically modified mouse models, providing a critical tool for understanding the role of that segment in health and disease.

DOI: https://doi.org/10.1007/s00424-013-1321-1

A primary culture system of mouse thick ascending limb cells with preserved function and uromodulin processing

Bob Glaudemans[1], Sara Terryn[2], Nadine Gölz[1], Martina Brunati[3], Angela Cattaneo[4], Angela Bachi[4], Lama Al-Qusairi[6], Urs Ziegler[5], Olivier Staub[6], Luca Rampoldi[3], and Olivier Devuyst[1,2*]

[1]Institute of Physiology, Zurich Center for Integrative Human Physiology, University of Zurich, Zurich, Switzerland; [2]Division of Nephrology, Université catholique de Louvain (UCL) Medical School, Brussels, Belgium; [3]Dulbecco Telethon Institute, Molecular Genetics of Renal Disorders Unit, and [4]Biomolecular Mass Spectrometry Unit, Division of Genetics and Cell Biology, San Raffaele Scientific Institute, Milan, Italy; [5]Center for Microscopy and Image Analysis (ZMB), University of Zurich; [6]Department of Pharmacology and Toxicology, University of Lausanne, Lausanne, Switzerland

ABSTRACT

The epithelial cells lining the thick ascending limb (TAL) of the loop of Henle perform essential transport processes and secrete uromodulin, the most abundant protein in normal urine. The lack of differentiated cell culture systems has hampered studies of TAL functions. Here we report a method to generate differentiated primary cultures of TAL cells, developed from microdissected tubules obtained in mouse kidneys. The TAL tubules cultured on permeable filters formed polarized confluent monolayers in ~12 days. The TAL cells remain differentiated and express functional markers such as uromodulin, NKCC2 and ROMK at the apical membrane. Electrophysiological measurements on primary TAL monolayers showed a lumen-positive transepithelial potential (+9.4±0.8 mV/cm^2) and transepithelial resistance similar to that recorded *in vivo*. The transepithelial potential is abolished by apical bumetanide and in primary cultures obtained from ROMK knockout mice. The processing, maturation and apical secretion of uromodulin by primary TAL cells is identical to that observed *in vivo*. The primary TAL cells respond appropriately to hypoxia, hypertonicity and stimulation by desmopressin, and they can be transfected. The establishment of this primary culture system will allow the investigation of TAL cells obtained from genetically modified mouse models, providing a critical tool for understanding the role of that segment in health and disease.

Keywords: Epithelial transport, NKCC2, ROMK, loop of Henle, TAL

INTRODUCTION

The mammalian kidney is characterized by a complex tubular segmentation, reflecting specialized functions and regulatory pathways. The thick ascending limb (TAL) of the loop of Henle plays essential roles in the reabsorption of sodium, the handling of divalent cations, and the urinary concentrating ability. The reabsorption of sodium by the TAL cells involves the apical, bumetanide-sensitive Na^+,K^+,$2Cl^-$-cotransporter NKCC2, organized in parallel with the renal outer medullary K^+ (ROMK) channel [16]. The K^+ recycling activity of ROMK contributes to the lumen-positive transepithelial potential, which favours the paracellular reabsorption of sodium and divalent cations in that segment [13,23]. The activity of NKCC2 in the TAL is regulated by the antidiuretic hormone arginine vasopressin (AVP), via type 2 receptors (V2R) [3].

In addition to high transport activity, the epithelial cells lining the medullary TAL are characterized by their ability to cope with hypertonicity and relative hypoxia. The osmoprotective response is ensured by multiple pathways that converge to the transcription factor tonicity-responsive enhancer binding protein (TonEBP) [7]. The high energy demands of medullary TAL cells are challenged by poor medullary blood flow [18]. This difficulty is balanced by the hypoxia-inducible factor (HIF) pathway, which plays a major role to protect the cells against oxygen deprivation [39].

The TAL cells are the exclusive production site of uromodulin (Tamm-Horsfall protein), the most abundant protein secreted in the normal urine [35]. The roles of uromodulin include protection against urinary tract infections [4]; prevention of calcium crystal aggregation [27]; and regulation of the activity of NKCC2 and/or ROMK [31,37]. Mutations in the *UMOD* gene that codes for uromodulin are responsible for defective processing of uromodulin in the TAL, leading to tubular

dysfunction and progressive renal failure [11,35]. Recently, genome wide association studies (GWAS) revealed that variants in *UMOD* are associated with the risk of developing chronic kidney disease in the general population [25]. There is thus a strong rationale to obtain a TAL cellular system able to decipher the role(s) of uromodulin in both monogenic diseases and complex disorders.

As compared with the proximal tubule, fewer cell lines derived from the TAL have been proposed. Techniques based on magnetic separation by antibodies [1,34], density gradient centrifugation [9,14,20], microdissection [8,42,44], and sieving [19,24] have been used to isolate primary TAL cells. Immortalized TAL cells have also been obtained from transgenic SV40 mice [6,10]. These culture systems are, to a variable extent, limited by insufficient purity and loss of terminal differentiation (lack of TAL markers). Furthermore, they have been insufficiently characterized in terms of transport and response to environment (hypoxia, osmotic stress) and hormonal stimulation. Since primary cultures were usually obtained from rat and rabbit kidney, they could not take advantage of genetically modified mouse models. Finally, to the best of our knowledge, none of the TAL cell systems has been shown to conserve the complex processing of uromodulin as observed *in vivo*.

We report here the establishment of a primary culture system based on pure TAL segments microdissected from mouse kidney and grown on permeable filters. These polarized monolayers display morphological features and critical functions of TAL cells *in vivo*, including electrophysiological properties and processing of uromodulin.

MATERIALS AND METHODS

Primary cell culture of mouse TAL cells

Primary cell cultures of mouse TAL (mTAL) cells were prepared using a modified version of previously described protocols [24,41]. Three to 6 week-old wild-type mice (C57/BL6 (Charles River, Suzbach, Germany), uromodulin knockout [30], ROMK knockout [28], and parvalbumin-EGFP [29] lines) were sacrificed with sevoflurane (Abbott Laboratories, Abbott Park, Illinois, USA). Kidneys were removed and placed into ice-cold HBSS dissection solution (Lonza, Verviers, Belgium), supplemented with 15 mM hepes (Lonza), 10 mM D-glucose (VWR International, Lucerne, Switzerland), 5 mM glycine (VWR International) and 1 mM L-alanine (Applichem GmbH, Darmstadt, Germany), pH 7.4, 325 mOsm/kg H_2O. Each kidney was cut along the midsagittal plane into two halves, and further into transverse sections. After removing the cortex and inner medulla, the outer medulla was cut into 1 mm-square pieces, followed by a 30-min treatment in dissection solution supplemented with 245 units/ml type-2 collagenase (Worthington Biochemical Corp, Lakewood, USA) and 96 µg/ ml soybean trypsin inhibitor (Sigma, St. Louis, USA). The collagenase-digested segments were sieved through a 250 µm filter (BVBA Prosep, Zaventem, Belgium) and collected on a 80 µm filter (BVBA) to obtain tubules longer than 100 µm. The sieved tubular segments were collected in 37^{o}C albumin solution (dissection solution supplemented with 1% (w/v) BSA (VWR International) and 96 µg/ml soybean trypsin inhibitor (Sigma)). The TAL tubules were viewed under a light microscope (Leica DM IL, Bensheim, Germany) and selected on the basis of morphology characteristics (Fig. 1A), using a glass pipet connected to a micromanipulator (Narishige International, London, UK). Pooled TAL segments (typically, ~50 collected) were placed onto 0.33 cm² collagen-coated PTFE filter

membranes (Transwell-COL, pore size 0.4 µm, Corning Costar, USA) in culture medium DMEM:F12 (Gibco-BRL, Breda, The Netherlands) supplemented with 15 mM HEPES (Gibco-BRL), 0.55 mM Na-pyruvate (Gibco-BRL), 0.01% (v/v) non-essential amino acids (Gibco-BRL), 2% (v/v) FBS (Lonza) and one batch of SingleQuots® (Lonza), pH 7.4 and incubated in a humidified chamber at 37°C – 5% CO_2. The medium was changed every 48 h. A confluent monolayer of TAL cells expanded from the tubular fragments after ~12 days.

When the cultures were close to forming confluent monolayers, the cells were cultured under low serum conditions (0.1% for 4-6 days) to allow maximal differentiation. Typically primary TAL cells were harvested, and apical medium was collected, after 4 days at low serum conditions. Following 0.04% (w/v) trypsin (Gibco-BRL) treatment, the primary TAL cultures could be passaged to either new 0.33 cm² collagen-coated PTFE filter membranes (1 to 6 dilution) or 24-well plastic culturing plates (Nunc™ Cell Culture 24-well MicroWell; 1 to 4 dilution).

SYBR Green real-time quantitative PCR

Total RNA was extracted from isolated segments and primary cultures using the RNAqueous^{R} kit (Applied Biosystems Inc, Foster city, USA), according to manufacturers protocol. The obtained RNA was subjected to DNase treatment and reverse transcriptased by using the iScript™ cDNA Synthesis Kit (Bio-Rad, München, Germany). RT-qPCR analyses were performed in duplo using 100 nM of both sense and anti-sense primers (Table 1) in a final volume of 20 µl using iQ™ SYBR Green Supermix (Bio-Rad) and an iCycler IQ System (Bio-Rad). The following PCR conditions were used: 94°C for 3 min, followed by 40 cycles of firstly 30 sec at 95°C, secondly 30 sec at 61°C and finally 1 min at 72°C. All amplicons

showed expected sizes and the dissociation curves showed one melting peak, ensuring the absence of a non-specific by-product or primer dimers. Glyceraldehyde 3-phosphate dehydrogenase (*Gapdh*) was used routinely as a reference gene, since preliminary experiments showed no significant differences with other reporter genes (*Cyclophilin, Hprt1, Actb, 36b4*). The relative changes in target gene/GAPDH mRNA ratio were determined by the formula: $2^{\Delta\Delta ct}$.

Antibodies

The following antibodies were used for immunostaining and/or immunoblotting: sheep anti-uromodulin (Meridian #K90071C) and rabbit anti-uromodulin (gift of Prof. F. Serafini-Cessi); rabbit anti-NKCC2 (Millipore #AB3562P); rabbit anti-ROMK (directed against a GST-fusion protein containing amino acids 342-391 of rat ROMK, and affinity-purified on maltose-binding protein comprising the same epitope. The specificity of the anti-ROMK antibodies has been validated on ROMK knockout mouse tissue (immunostaining) and inducible cell lysates (immunoblotting) (Johannes Loffing and Olivier Staub, personal communication); rabbit anti-AQP1 (Millipore #AB2219); rabbit anti-AQP2 (Sigma #A7310); and monoclonal mouse anti-β-actin (Sigma #A5441).

Immunostaining

Confluent monolayers of primary cultured TAL were fixed for 10 min by 4% (w/v) paraformaldehyde (Sigma), permeabilized for 5 min in 0.2% (v/v) Triton X-100 (Sigma) and incubated for 1h using 3% (v/v) blocking serum. The primary antibody was diluted in PBS (Gibco-BRL) containing 2% (w/v) BSA (VWR International) and incubated for 1 h at room temperature. After four PBS washing steps, monolayers

were incubated with Alexa Fluor® secondary antibodies (Invitrogen, Breda, the Netherlands: goat anti-rabbit alexa 633 (A-21071); donkey anti-sheep alexa 633 (A-11015)) for 30 min at room temperature. After PBS washing, filters were cut from the holder and mounted in Prolong Gold Anti-fade reagent (Invitrogen). The same procedure was used to stain paraffin-embedded sections from mouse kidneys. Sections were viewed using a LSM510Meta Confocal microscope (Carl Zeiss, Oberkochen, Germany), with an x63/1.4 Plan-Apochromat oil-immersion objective.

Immunoblotting

Immunoblotting was performed as described previously [17]. In short, mouse kidneys, isolated segments and confluent primary mTAL monolayers were solubilised in lysis buffer (1mM EDTA (Merck), 20 mM imidazole (AppliChem GmbH, Darmstadt, Germany), 250 mM sucrose (VWR)) containing Complete Mini protease inhibitors (Roche Diagnostics, Brussels, Belgium), followed by a brief sonication and centrifugation at 16,000 g for 1 min at 4°C. Protein concentrations were determined using the bicinchoninic acid (BCA) protein assay (Pierce, Aalst, Belgium). Samples were thawed on ice, normalized for protein levels, diluted in Laemmli sample buffer (Bio-Rad) and separated by sodium dodecyl sulphate (SDS) polyacrylamide gel electrophoresis (PAGE) and blotted onto nitrocellulose. Membranes where blocked for 30 min in 5% w/v non-fat dry milk solution at room temperature, followed by overnight incubation at 4°C with primary antibodies. Thereafter blots where washed and incubated with peroxidase-conjugated secondary antibodies (rabbit anti-sheep HRP, P0163; goat anti-rabbit HRP, P0488; both from Dako, Glostrup, Denmark), washed and visualized by Immun-Star™ enhanced chemiluminescence (Bio-Rad).

Immunoblots were quantified by densitometry using ImageJ (Image Processing Program, NIH, USA) software.

Transmission electron microscopy

Primary TAL cells on permeable filter supports were fixed with 0.8% (m/v) formaldehyde (EMS, München, Germany) and 2.5% (m/v) glutaraldehyde (Fluka, Buchs SG, Switzerland) buffered in 0.1 M sodium cacodylate (Merck) for 30 min, followed by additional overnight incubation in 0.1 M sodium cacodylate buffer. The cells were postfixed for 30 min in 1% (m/v) osmium tetraoxide (EMS) buffered in 0.1 M sodium cacodylate, dehydrated in a graded series of ethanol and propylene oxide (Fluka) and embedded in epoxy resin (Fluka). Sections were prepared using an ultracryomicrotome (UltracutUCT, Leica, Bensheim, Germany). Semi-thin (200 μm) sections stained with toluidine blue (Fluka) were analysed by light microscopy. Ultrathin (65 nm) sections were mounted on Athene schlitz copper grids (Plano, Wetzlar, Germany), contrasted with uranyl acetate dihydrate (Fluka) and lead citrate (Merck) and investigated by use of a Philips CM100 (Eindhoven, The Netherlands) transmission electron microscope.

Electrophysiology

Confluent primary TAL monolayers (from wild-type and ROMK knockout mice) on filters were subjected to simultaneous transepithelial potential difference (V_{te}) and resistance (R) measurements using an EVOM-G potentiometer (WPI, Sarasota, USA), and Endohm 6 electrodes (WPI). The effect of NKCC2 inhibition was tested after incubation with 100 μM bumetanide (Sigma) for 5 min.

Uromodulin recovery and shedding experiments

Confluent monolayers of TAL cells grown on filter support were used for uromodulin recovery and shedding experiments. After collection of the last 48-h apical supernatant, the cells were washed twice with 37 ^{o}C PBS, followed by application of 200 µl of fresh medium to the apical compartment. Samples (20 µl) of apical medium were taken after 2, 4, 8, 12 and 16 h to assess uromodulin level by immunoblotting. The influence of apical protease activity on the shedding of uromodulin was assessed by treating primary TAL monolayers with a protease inhibitor cocktail (PIC, P8340, Sigma) (1:1000 v/v in apical medium) for 16h, after which uromodulin concentration in the apical medium was measured by immunoblotting.

Hypoxic and hypertonic treatment of primary TAL cells

To address the hypoxic response, mouse primary TAL cells were cultivated at 37 ^{o}C for 24 h at low oxygen (0.2%) in a Ruskinn Invivo^{2} 400 incubator (Bridgend, United Kingdom) and compared to cells cultured at normal oxygen (21%) concentration. To study the hypertonic response, primary TAL cells were cultured at 37 ^{o}C for 6 h under isotonic (320 mOsm) or hypertonic (480 mOsm) conditions (by addition of NaCl to the medium). Following the exposure to hypoxia or hypertonic conditions, the cells were harvested to extract mRNA and perform RT-qPCR.

Treatment with DDAVP and cAMP assay

Primary TAL cultures were stimulated by 10^{-8} M of V2 receptor agonist DDAVP (Sigma) for 5 min at room temperature at both the apical and basolateral side of the filter support. The dose-response curve was obtained by applying different concentration of dDAVP (10^{-7} to 10^{-12} M) at the basolateral side. The cAMP

concentration was determined by use of the DetectX® Cyclic AMP enzyme immunoassay kit (Arbor Assays, Ann Arbor, USA), according to manufacturers recommendations.

Transfection of primary TAL monolayers

Transfections were carried out for 24h in primary mTAL cells reaching 90% of confluence. After transfer in medium without antibiotics, cells were transfected with 50nM of BLOCK-iT™ Alexa555 Red Fluorescent Oligo (fluorescence-based indication of transfection efficiency) diluted in Opti-MEM containing Lipofectamine™ RNAiMAX (Invitrogen, Breda, The Netherlands). The medium was changed 6h after transfection. Control cells were transfected with a non-fluorescent SilencerRNegative control siRNA (Invitrogen) in the same conditions.

The RNA interference experiment against UMOD was performed with small interference RNA (siRNA) with 21 nucleotides (Silencer® Select Pre-designed siRNA; Ambion). To knockdown the endogenous UMOD expression, 3 different double-strand siRNA (50nM) were introduced into prTAL cells using Lipofectamine™ RNAiMAX (Invitrogen). Control cells were transfected with a non-fluorescent SilencerRNegative control siRNA (Invitrogen) in the same conditions. Total RNA was extracted 48 h after transfection using RNAqueous®-Micro kit, prior to RT-qPCR analyses for the expression of *Umod* (target) and *Clcn5* (non-specific gene expressed in TAL).

Protein precipitation and deglycosylation

Proteins present in the extracellar medium (75µl) or mouse urine (5µl) were precipitated by adding 4 volumes of acetone to the samples. The pellets were dried for

30 min and resuspended in PBS. Samples were deglycosylated using peptide-*N*-(*N*-acetyl-β-glucosaminyl) asparagine amidase (PNGase F) (New England Biolabs), according to the manufacturer recommendations. In short, each sample was incubated for 15 min at 55°C in denaturing buffer, followed by 1 h incubation at 37°C in G7 buffer containing 1% NP-40 and 0.5 µl of PNGase F.

Mass spectrometry analysis

Deglycosylated proteins or urinary samples were alkylated in 55 mM IAA (Iodoacetamide) for 20 min at room temperature, separated on 8% acrylamide SDS–PAGE and stained with Coomassie Brilliant Blue (Sigma–Aldrich).

nLC-MS/MS analysis: Band of interest was excised from gel, subjected to reduction (10 mM DTT) alkylation (55 mM IAA) and digestion with Asp-N (Roche) [38]. Peptide mixtures were concentrated, desalted [36] and analyzed on a LTQ-Orbitrap mass spectrometer (Thermo Fisher Scientific) equipped with a nanoelectrospray ion source (Proxeon Biosystems, Odense, Denmark) and coupled on line to an Easy-nLC (Proxeon). Peptide separations occurred on a RP homemade 25 cm reverse-phase spraying fused silica capillary column (75 μm i.d. × 25 cm), packed with 3 μm ReproSil-Pur C18-AQ (Dr. Maisch GmbH, Germany). A gradient of eluents A (H_2O with 2% v/v ACN, 0.5% v/v acetic acid) and B (80%ACN with 0.5% v/v acetic acid) was used to achieve separation, from 4% B (at 0 min 0.15 μL/min flow rate) to 70% B (in 65 min, 0.15 μL/min flow rate).

MS and MS/MS spectra were acquired selecting the ten most intense ions per survey spectrum acquired in the orbitrap from *m*/*z* 300-1750 with 60.000 resolution. Target ions selected for the MS/MS were fragmented in the ion trap and dynamically excluded for 120s. Target value were 1,000,000 for survey scan and 100,000 for

MS/MS scan. For accurate mass measurements, the lock-mass option was employed [33] selecting the 371.1012 amu ion.

Database search: The acquired MS files were converted into peaklist (.msm files) and analyzed using Mascot (Matrix Science, London, UK; version 2.2.0.7) searching against the uniprot_cp_mus_2013_02 database (50287 sequences; 24229016 residues). Searches were performed using semi_Asp-N cleavage option; a fragment ion mass tolerance of 0.60 Da and a parent ion tolerance of 5.0 ppm. Carbamidomethylation of cysteine was specified as a fixed modification; oxidation of methionine, asparagine deamidation and acetylation of the N-terminus of proteins were specified as variable modifications.

Statistical analysis

All values are expressed as mean ± SEM. Overall statistical analyses were performed by Student's t-test. $P<0.05$ is considered statistically significant.

RESULTS

Microdissection and isolation of pure TAL tubules

The outer medulla from 4 to 6-week old mouse kidneys was dissected and treated with collagenase to obtain single tubule fragments. These segments included some glomeruli and proximal convoluted tubules (PCT), and numerous proximal straight tubules (PST), TAL and connecting tubules/collecting ducts (CNT/CD) (Figure 1). The tubular segments could be distinguished by simple morphological criteria (Fig. 1A). Both the PCT and PST showed a large diameter (~60μm). The PCT presented many convolutions, with an open lumen, while the PST are straight, darker, and have a collapsed v-shaped lumen. The TAL tubules showed a smaller diameter (~30μm) and smooth structure, and they rarely presented an open lumen. The CNT and CD tubules had a light-coloured cobblestone appearance and branching.

We collected 50-60 of each of these segments to investigate the expression of segment-specific marker genes by using reverse transcriptase PCR (RT-PCR). NKCC2 and uromodulin (UMOD) were expressed in the TAL, but not in other segments. In contrast, aquaporin-1 (AQP1) and N-glutamine transporter 3 (SNAT3); aquaporin-2 (AQP2); and podocin were not detected in the TAL tubules (Figs. 1B,C). The TAL preparations were also negative for the Na^+-Cl^- cotransporter NCC, a marker of the distal convoluted tubule (with positive control obtained from the parvalbumin-EGFP mouse; data not shown). Real-time qPCR was used to confirm the enrichment of microdissected fragments with their respective markers, including NKCC2 and UMOD for the TAL (Fig. 1C). Altogether, these data indicate that the microdissection and isolation procedure yielded a high enrichment of pure TAL segments.

Culture of TAL tubules on collagen-coated filter supports

Following microdissection, ~50 tubules were placed on a filter support to obtain the primary cultures (Figure 2). The cultures (n= ~10 per kidney) were seeded within 2 h after dissection. The formation of small cell islands, usually starting at the end of the tubules, was observed during the first 4-5 days. These islands joined after ~10 days, to form confluent cultures on filters at ~12 days after seeding (Fig. 2A).

Morphological examination of confluent primary TAL cultures grown on filters revealed well-polarized monolayers of cuboidal epithelial cells (9-10 μm high) on transverse sections (Fig. 2B). Ultrastructural examination by transmission electron microscopy (Figs. 2C-F) showed that the cells are characterized by short apical microvilli (Figs. 2C,D), well-developed rough endoplasmic reticulum (Fig. 2D), large basolateral and smaller size luminal mitochondria (Figs. 2C,E), and tight junctions and packed filopodia (Figs. 2C,F). Of note, dome formation was not observed in these TAL cell cultures either grown on filters or on plastic plates.

Expression and processing of uromodulin in primary TAL cells

The primary TAL cultures were analyzed for the expression of functional markers, using confocal microscopy (Figure 3) and immunoblotting experiments (Figure 4). A strong immunostaining for uromodulin and NKCC2 was observed in the TAL monolayers (Fig. 3A). The staining partly overlapped, as NKCC2 is located at or in vesicles close to the apical membrane, while uromodulin presented additional staining in the extracellular compartment, with formation of large filaments (Figs. 3A,C). The apparent patchy staining of uromodulin was in fact reflecting the undulant topology of the primary TAL monolayers as shown on the ZY-stack image (Fig. 3A). This staining pattern was similar to the one observed in mouse kidney, where both

uromodulin and NKCC2 localize to apical membrane of the TAL (Fig. 3A, lower panel). The primary TAL cells also expressed a strong, apical staining for ROMK (Fig. 3B). Distinctive uromodulin filaments were detected on the apical surface of primary TAL cells obtained from wild-type kidneys, and absent in cells obtained from uromodulin knockout kidneys (Fig. 3C).

Immunoblotting confirmed the expression of NKCC2 in microdissected TAL tubules and primary TAL cultures, while AQP1 and AQP2 were absent (Fig. 4A). A consistent expression of NKCC2 and uromodulin was detected in primary TAL cells after 4 days on low serum conditions (Fig. 4B). RT-qPCR experiments showed that the primary TAL cultures expressed high levels of the medulla-specific NKCC2F variant and lower levels of the NKCC2A variant (95 ± 26% and 5 ± 0%, respectively, n=9), with no amplification of the cortex-specific NKCC2B variant (data not shown).

We next investigated whether uromodulin is appropriately sorted and secreted, as occurs *in vivo*. Apical wash-out experiments showed a progressive secretion of uromodulin in the apical medium, that was apparent 4-8 h after changing the medium (Fig. 4C). The secretion of uromodulin from the TAL into the urine is mediated by a conserved proteolytic cleavage *in vivo* [38]. Accordingly, the application of a protease inhibitor cocktail (PIC) to the luminal pole of the primary TAL monolayers resulted in a 65% reduction in the apical release of uromodulin (Fig. 4D).

Deglycosylation of uromodulin released in the apical medium yielded a main short isoform, similar in size to the variant detected in mouse urine, and one at higher molecular mass (Figure 5). Analysis of the short isoform by mass spectrometry analysis confirmed that uromodulin cleavage in the primary TAL cells is similar to that occurring *in vivo*, since the vast majority of identified peptides have the same C-terminus (F588 residue) as urinary uromodulin [38] (Fig. 5).

Electrophysiological characteristics of primary TAL cells

Transepithelial potential (V_{te}) difference and electrical resistance (R) were measured in order to seek whether the characteristic, lumen-positive voltage observed *in vivo* is preserved in the primary TAL monolayers (Table 2). These measurements showed that V_{te} averaged 9.4±0.8 mV (lumen-positive) and R, 73±12 ohm.cm^2 across the confluent primary TAL monolayers (n=15).

The transport activity of the bumetanide-sensitive NKCC2 cotransporter and the recycling of K^+ via ROMK are both essential for generating the lumen-positive V_{te} in TAL cells. The preservation of the latter functional coupling and its role in maintaining V_{te} in TAL primary cells was confirmed by two different approaches (Figure 6). Treatment with bumetanide (100 µM) induced a strong decrease in V_{te} (from 11.5±1.4 to 2.2±0.6 mV, control vs. treatment, n=7; p=0.01), which was reversible on washout (back to 9.8±1.3 mV) (Fig. 6A). To investigate the K^+ recycling influence and the applicability of the method to various mouse strains, we generated TAL primary cultures from ROMK knockout mice [28]. The primary TAL cells obtained from these mice displayed normal growth rate and morphology, but presented a significant decrease in V_{te} (9.6±0.5 vs. 2.4±0.2 mV, control vs. ROMK KO, n=6; p=0.0010) (Fig. 6B).

Primary TAL cells respond to DDAVP, hypoxia and hypertonicity

We tested whether the primary TAL cells respond to stimuli influencing the activity of the TAL *in vivo*. The primary TAL cells were shown to express the arginine vasopressin receptor 2 (AVPR2), like in mouse kidney (Fig. 6C). Stimulation of the monolayers with the V2R agonist desmopressin (DDAVP) induced a dose-dependent increase in intracellular cAMP concentration with a maximal effect reached at ~100

nM DDAVP, while a half-maximal effect (EC50) was obtained at ~5 nM DDAVP (Fig. 6C). The effect of DDAVP was polarized, as shown by the difference in cAMP concentrations obtained after DDAVP applied on the apical vs. basolateral side (7.8±2.2 vs. 119.5±21.2 pmol/mL, respectively; n=6, p<0.01) (Fig. 6D).

The effect of HIF1α and target genes such as pyruvate dehydrogenase 2 (PHD2) and glucose transporter (GLUT1) was studied following a 24-h incubation of the TAL cultures at low (0.2%) vs. control (21%) oxygen concentration (Fig. 6E). Compared to control, the mRNA expression levels of PHD2 (1.00±0.16 vs. 5.16±0.96, respectively; n=4, p=0.03) and GLUT1 (1.00±0.17 vs. 2.32±0.29, respectively; n=4, p=0.006) were significantly increased, whereas that of pyruvate dehydrogenase 1 (PHD1) was unchanged (1.00±0.11 vs. 0.90±0.12; n=4). Hypertonicity is known to stimulate transcription activator TonEBP and target genes such as heat shock protein 70 (HSP70) and aldose reductase (AR) in the TAL *in vivo*. Exposure of the TAL cell cultures to hypertonic medium (480 mOsm) for 6h yielded robust increase in the mRNA expression levels of TonEBP (1.00±0.07 vs. 2.16±0.31; n=4, p=0.03), HSP70 (1.00±0.05 vs. 7.96±0.65; n=4, p=0.002) and AR (1.00±0.05 vs. 25.96±3.20; n=4, p=0.004) (Fig. 6F). These data demonstrate that the primary TAL cells respond appropriately to hormonal and environmental stimuli operating in the TAL *in vivo*.

Transfectability of the primary TAL cells

The possibility to transfect the primary TAL cells (Figure 7) was demonstrated using lipofectamin-mediated internalization of an Alexa555-conjugated siRNA, which yielded a fluorescent signal in ~50% of the cells (Fig. 7A). A similar approach was used to show the possibility to specifically target endogenous uromodulin with siRNA in primary TAL cells (Fig. 7B).

DISCUSSION

In this report, we describe a technique that combines microdissection, enzymatic digestion, differential sieving and culture on collagen-coated filters to obtain pure, differentiated medullary TAL primary cultures from mice. These cells (i) are polarized and show morphological features of the TAL; (ii) express NKCC2, ROMK and uromodulin; (iii) display a lumen-positive transepithelial voltage that is sensitive to bumetanide and likewise depends on ROMK activity; (iv) respond to stimuli such as hypoxia, hypertonicity and vasopressin; and (v) process and secrete uromodulin with typical features observed *in vivo*.

The technique described here yields confluent monolayers of primary TAL cells approximately 12 days after seeding, with ~10 inserts per mouse kidney. The primary TAL cells show morphological features, including cuboïdal appearance, height averaging 8-9 μm, tight junctional belts, large basal and smaller luminal mitochondria, and sub-apical vesicles similar to the ultrastructural features of native rodent TAL [2]. The primary TAL cells display a consistent expression of NKCC2 and uromodulin, with the latter identified at the luminal membrane and also as filaments on the apical surface of the cells. This apical distribution of NKCC2, ROMK and uromodulin in the TAL cells is similar to the *in vivo* situation. Furthermore, the primary TAL cultures express high levels of the medulla-specific NKCC2F, lower levels of NKCC2A, and no cortical NKCC2B variant, in line with the micro-dissected medullary TAL segments used to generate the cultures [21].

The primary TAL cells show a high level of expression of uromodulin, that is processed intracellularly, sorted to the apical membrane and released in the apical medium, mostly through the same proteolytic cleavage occurring *in vivo* (Figs. 3 and 4). To our knowledge, this is the first cellular system in which the processing of

uromodulin is evidenced to be similar to that observed *in vivo*. Uromodulin has been recently pointed as a urinary biomarker relevant for renal function, chronic kidney disease and hypertension [35]. Uromodulin is a ~105 kD glycoprotein containing 616 amino acids with 48 cysteine residues, three epidermal growth factor (EGF)-like domains and a zona pellucida (ZP) domain, found in many extracellular proteins, as well as a glycosylphosphatidylinositol (GPI)-anchoring site. After trafficking and maturation in TAL-lining cells, uromodulin reaches the apical plasma membrane to be cleaved by unknown proteases and assembled in the urine as large polymers [43]. Our studies demonstrate that the polarized secretion of uromodulin in primary TAL cells yields such filaments, made of secretory variants exactly similar to those observed in mouse urine. The mTAL cellular system described here will thus be valuable to further investigate the complex processing and function of uromodulin. The possibility to transfect the primary TAL cells, as shown by lipofectamin-mediated internalization of siRNAs (Fig. 7), will be particularly important in that context.

Electrophysiological recordings of primary TAL cells demonstrated an essential feature of the TAL segment, i.e. a lumen-positive V_{te} that depends on the activity of NKCC2 and ROMK. The V_{te} recorded at baseline is comparable to values observed by microperfusion studies on isolated perfused mouse TAL tubules [12,23]. Furthermore, Vte was reversibly abolished by bumetanide and also significantly attenuated in primary TAL cultures obtained from ROMK KO mice. On one hand, the latter result confirms the functional link between the lumen-positive voltage and the K^+ recycling through ROMK [22]. On the other hand, this experiment serves as a proof-of-principle demonstration of the usefulness of the method to investigate transgenic mouse models relevant for TAL function. It must be noted that we could

not observe dome formation with the primary TAL cells cultured on plastic, which could suggest that the water impermeability of the TAL is preserved in this differentiated culture system.

Vasopressin signaling via the V2R-cAMP pathway is a strong activator of NKCC2 in the TAL [3,32]. We show here that V2R is expressed in the primary TAL cultures and that a dose-dependent increase in cAMP follows treatment with DDAVP. These results are in line with previous observations in TAL micropuncture studies and microdissected TAL segments, with similar dose-dependance of cAMP generation to DDAVP [5,15]. The cells lining the medullary TAL are particularly sensitive to oxygen deprivation in view of their high metabolic activity [18]. To assess whether primary TAL cells respond appropriately to hypoxic conditions, we measured the mRNA levels of hypoxia target genes. Both the prolyl 4-hydroxylase domain protein PHD2 and the glucose transporter GLUT1 were significantly increased in the primary TAL cells under hypoxic conditions, contrasting with the stable expression of the PHD1 isoform. These results are in line with *in vivo* experiments using kidneys of hypoxic mice [40]. *In vivo*, medullary TAL cells are protected against the deleterious effects of hypertonicity by transcription activator TonEBP and target genes HSP70 and AR [7,26]. We observed a similar upregulation in primary TAL cells exposed to hypertonic treatment.

The availability of a differentiated TAL cellular system obtained from mouse kidney opens new perspectives for the analysis of the role played by the TAL in health and disease.

ACKNOWLEDGEMENTS

The authors would like to thank Gery Barmettler, Soline Bourgeois, Huguette Debaix, David Hoogewijs and Klaus Marquardt for assistance and helpful suggestions. Prof. Jan Loffing kindly provided the parvalbumin-EGFP mouse. The uromodulin knockout mouse was developed and kindly provided by Prof. X-R. Wu.

These studies were supported in part by the European Community's Seventh Framework Programme (FP7/2007-2013) under grant agreement n° 246539 (Marie Curie) and grant n° 305608 (EURenOmics); an Action de Recherche Concertée (ARC, Communauté Française de Belgique); the FNRS and FRSM; the Inter-University Attraction Pole (IUAP, Belgium Federal Government); the NCCR Kidney.CH program (Swiss National Science Foundation); the Gebert Rüf Stiftung (Project GRS-038/12); and the Swiss National Science Foundation 31003A-125422/1 (to OS) and 310030-146490 (to OD).

The authors declare no competing interests.

REFERENCES

1. Allen ML, Nakao A, Sonnenburg WK, et al (1988) Immunodissection of cortical and medullary thick ascending limb cells from rabbit kidney. Am J Physiol 255: F704-F710

2. Allen F, Tisher CC (1976) Morphology of the ascending thick limb of Henle. Kidney Int 9: 8-22

3. Ares GR, Caceres PS, Ortiz PA (2011) Molecular regulation of NKCC2 in the thick ascending limb. Am J Physiol Renal Physiol 301: F1143-F1159

4. Bates JM, Raffi HM, Prasadan K, et al (2004) Tamm-Horsfall protein knockout mice are more prone to urinary tract infection: rapid communication. Kidney Int 65: 791-797

5. Baudouin-Legros M, Bouthier M, Teulon J. Arginine]vasopressin hydrolyses phosphoinositides in the medullary thick ascending limb of mouse nephron. Pflugers Arch 425: 381-389

6. Bourgeois S, Rossignol P, Grelac F, et al (2003) Differentiated thick ascending limb (TAL) cultured cells derived from SV40 transgenic mice express functional apical NHE2 isoform: effect of nitric oxide. Pflugers Arch 446: 672-683

7. Burg MB, Ferraris JD, Dmitrieva NI (2007) Cellular response to hyperosmotic stresses. Physiol Rev 87: 1441-1474

8. Burg M, Green N, Sohraby S, Steele R, Handler J (1982) Differentiated function in cultured epithelia derived from thick ascending limbs. Am J Physiol 242: C229-C233

9. Chamberlin ME, LeFurgey A, Mandel LJ (1984) Suspension of medullary thick ascending limb tubules from the rabbit kidney. Am J Physiol 247: F955-F964

10. Chang CT, Hung CC, Tian YC, Yang CW, Wu MS (2007) Ciclosporin reduces paracellin-1 expression and magnesium transport in thick ascending limb cells. Nephrol Dial Transplant 22: 1033-1040

11. Dahan K, Devuyst O, Smaers M, et al (2003) A cluster of mutations in the UMOD gene causes familial juvenile hyperuricemic nephropathy with abnormal expression of uromodulin. J Am Soc Nephrol 14: 2883-2893

12. Di Stefano A, Jounier S, Wittner M (2001) Evidence supporting a role for KCl cotransporter in the thick ascending limb of Henle's loop. Kidney Int 60: 1809-1823

13. Di Stefano A, Roinel N, de Rouffignac C, et al (1993) Transepithelial Ca2+ and Mg2+ transport in the cortical thick ascending limb of Henle's loop of the mouse is a voltage-dependent process. Ren Physiol Biochem 16: 157-166

14. Drugge ED, Carroll MA, McGiff JC (1989) Cells in culture from rabbit medullary thick ascending limb of Henle's loop. Am J Physiol 256: C1070-C1081

15. Dublineau I, Elalouf JM, Pradelles P, et al (1989) Independent desensitization of rat renal thick ascending limbs and collecting ducts to ADH. Am J Physiol 256: F656-663

16. Devuyst O (2008) Salt wasting and blood pressure. Nat Genet 40: 495-496

17. Devuyst O, Christie PT, Courtoy PJ, et al (1999) Intra-renal and subcellular distribution of the human chloride channel, CLC-5, reveals a pathophysiological basis for Dent's disease. Hum Mol Genet 8: 247-257

18. Eckardt KU, Bernhardt WM, Weidemann A, et al (2005) Role of hypoxia in the pathogenesis of renal disease. Kidney Int Suppl 2005; 99: S46-S51

19. Eng B, Mukhopadhyay S, Vio CP, et al (2007) Characterization of a long-term rat mTAL cell line. Am J Physiol Renal Physiol 293: F1413-F1422

20. Eveloff J, Haase W, Kinne R (1980) Separation of renal medullary cells: isolation of cells from the thick ascending limb of Henle's loop. J Cell Biol 87: 672-681

21. Gamba G, Friedman PA (2009) Thick ascending limb: the Na(+):K (+):2Cl (-) co-transporter, NKCC2, and the calcium-sensing receptor, CaSR. Pfluegers Arch 458: 61-76

22. Hebert S (1995) An ATP-regulated inwardly rectifying potassium channel from rat kidney. Kidney Int 48: 1010–1016

23. Hebert SC, Culpepper RM, Andreoli TE (1981) NaCl transport in mouse medullary thick ascending limbs. I. Functional nephron heterogeneity and ADH-stimulated NaCl cotransport. Am J Physiol 241: F412-431

24. Jans F, Vandenabeele F, Helbert M, et al (2000) A simple method for obtaining functionally and morphologically intact primary cultures of the medullary thick ascending limb of Henle's loop (MTAL) from rabbit kidneys. Pflugers Arch 440: 643-651

25. Köttgen A (2010) Genome-wide association studies in nephrology research. Am J Kidney Dis 56: 743-758

26. Kwon MS, Lim SW, Kwon HM (2009) Hypertonic stress in the kidney: a necessary evil. Physiology (Bethesda) 24: 186-191

27. Liu Y, Mo L, Goldfarb DS, et al (2010) Progressive renal papillary calcification and ureteral stone formation in mice deficient for Tamm-Horsfall protein. Am J Physiol Renal Physiol 299: F469-F478

28. Lu M, Wang T, Yan Q, et al (2002) Absence of small conductance K+ channel (SK) activity in apical membranes of thick ascending limb and cortical collecting duct in ROMK (Bartter's) knockout mice. J Biol Chem 277: 37881-37887

29. Meyer AH, Katona I, Blatow M, et al (2002) In vivo labeling of parvalbumin-positive interneurons and analysis of electrical coupling in identified neurons. J Neurosci 22: 7055-7064

30. Mo L, Zhu XH, Huang HY, Shapiro E, Hasty DL, Wu XR (2004) Ablation of the Tamm-Horsfall protein gene increases susceptibility of mice to bladder colonization by type 1-fimbriated Escherichia coli. Am. J Physiol Renal Physiol 286: 795-802

31. Mutig K, Kahl T, Saritas T, et al (2011) Activation of the bumetanide-sensitive Na+,K+,2Cl- cotransporter (NKCC2) is facilitated by Tamm-Horsfall protein in a chloride-sensitive manner. J Biol Chem 286: 30200-30210

32. Mutig K, Paliege A, Kahl T, Jöns T, Müller-Esterl W, Bachmann S (2007) Vasopressin V2 receptor expression along rat, mouse, and human renal epithelia with focus on TAL. Am J Physiol Renal Physiol 2007; 293: F1166-F1177

33. Olsen JV, de Godoy LM, Li G, et al (2005) Parts per million mass accuracy on an Orbitrap mass spectrometer via lock mass injection into a C-trap. Mol Cell Proteomics 12: 2010–2021

34. Pizzonia JH, Gesek FA, Kennedy SM, Coutermarsh BA, Bacskai BJ, Friedman PA (1991) Immunomagnetic separation, primary culture, and characterization of cortical thick ascending limb plus distal convoluted tubule cells from mouse kidney. In Vitro Cell Dev Biol 27A: 409-416

35. Rampoldi L, Scolari F, Amoroso A, et al (2011) The rediscovery of uromodulin (Tamm-Horsfall protein): from tubulointerstitial nephropathy to chronic kidney disease. Kidney Int 80: 338-347

36. Rappsilber J, Ishihama Y, Mann M (2003) Stop and go extraction tips for matrix-assisted laser desorption/ionization, nanoelectrospray, and LC/MS sample pretreatment in proteomics. Anal Chem 75: 663-70

37. Renigunta A, Renigunta V, Saritas T, Decher N, Mutig K, Waldegger S. (2011) Tamm-Horsfall Glycoprotein interacts with Renal Outer Medullary Potasium Channel ROMK2 and regulates its function. J Biol Chem 286: 2224-2235

38. Santambrogio S, Cattaneo A, Bernascone I, et al (2008) Urinary uromodulin carries an intact ZP domain generated by a conserved C-terminal proteolytic cleavage. Biochem Biophys Res Commun 370: 410-413

39. Schley G, Klanke B, Schödel J, et al (2011) Hypoxia-inducible transcription factors stabilization in the thick ascending limb protects against ischemic acute kidney injury. J Am Soc Nephrol 22: 2004-2015

40. Stiehl DP, Wirthner R, Koditz J, et al (2006) Increased prolyl 4-hydroxylase domain proteins compensate for decreased oxygen levels. Evidence for an autoregulatory oxygen-sensing system. J Biol Chem 281: 23482-23491

41. Terryn S, Jouret F, Vandenabeele F, et al (2007) A primary culture of mouse proximal tubular cells, established on collagen-coated membranes. Am J Physiol Renal Physiol 293: F476-485.

42. Valentich JD, Stokols MF (1986) An established cell line from mouse kidney medullary thick ascending limb. I. Cell culture techniques, morphology, and antigenic expression. Am J Physiol 251: C299-C311

43. Wiggins RC (1987) Uromucoid (Tamm-Horsfall glycoprotein) forms different polymeric arrangements on a filter surface under different physicochemical conditions. Clin Chim Acta 162: 329-340

44. Wu MS, Bens M, Cluzeaud F, Vandewalle A (1994) Role ofF-actin in the activation of Na(+)-K(+)-Cl- cotransport by forskolin and vasopressin in mouse kidney cultured thick ascending limb cells. J Mernbr Bioi 142: 323-336

Table 1. Primers used in real-time RT-PCR analyses.

Gene product	Forward primer (5'-3')	Reverse primer (5'-3')	PCR bp	Efficiency
Arl15	TCC AGA ATG CCG TTT TGA AT	CAT CCT CTG AAG AGG CAC TGT	126	1.01 ± 0.03
Aqp1	GCT GTC ATG TAC ATC ATC GCC CAG	AGG TCA TTG CGG CCA AGT GAA T	107	0.99 ± 0.02
Aqp2	TCA CTG GGT CTT CTG GAT CG	CGT TCC TCC CAG TCA GTG T	147	1.03 ± 0.04
Avpr2	GGA AAT GGC AGT GGG GTA TT	GGC ACC AGA CTG GCA TGT AT	164	0.98 ± 0.04
Clcn5	TGG AGG AGC CAA TCC CTG GTG T	AGA AAG CAT CGC TCA CAC TG	156	1.01 ± 0.03
Glut1	TCT CTG TCG GCC TCT TTG TT	GCA GAA GGG CAA CAG GAT AC	380	NT
Hsp70A1	ACC ACC TAC TCG GAC AAC CA	CGA AGG TCA CCT CGA TCT GT	151	1.02 ± 0.03
Kcnj1	CCG TGT TCA TCA CAG CCT TCT T	CCG TAA CCT ATG GTC ACT TGG G	190	1.03 ± 0.03
Phd1	TTG CCT GGG TAG AAG GTC AC	GCT CGA TGT TGG CTA CCA CT	306	NT
Phd2	AGC CAT GGT TGC TTG TTA CC	CTC GCT CAT CTG CAT CAA AA	299	NT
Podocin	GTC TAG CCC ATG TGT CCA AA	CCA CTT TGA TGC CCC AAA TA	162	1.02 ± 0.03
Slc12a1 A	TGG GTT GTC AAC TTC TGC AA	AGC AAA GAT CAA GCC TAT TGA CC	118	NT
Slc12a1 B	ACA GGT TTG TCC ACC TCT GC	AGC AAA GAT CAA GCC TAT TGA CC	120	NT
Slc12a1 F	ATT GGC CTG AGC GTA GTT GT	AGC AAA GAT CAA GCC TAT TGA CC	150	0.99 ± 0.04
Snat3	ATT GGA GCC ATG TCC AGC TA	GGC AGA ATG ATG GTG ACA GA	149	0.98 ± 0.02
TonEBP	GCA AGG CTA TGC AAG TGG AG	GTC CTC AGG TGG TGG TGA G	152	0.97 ± 0.04
Umod	TTG CGA AGA ATG CAG GGT AG	TGG CAC TTT CTG AGG GAC AT	156	1.01 ± 0.02
Actb	TGC CCA TCT ATG AGG GCT AC	CCC GTT CAG TCA GGA TCT TC	102	1.02 ± 0,02
Cyclophilin	CGT CTC CTT CGA GCT GTT TG	CCA CCC TGG CAC ATG AAT C	139	1.02 ± 0.02
Gapdh	TGC ACC ACC AAC TGC TTA GC	GGA TGC AGG GAT GGG GGA GA	176	1.04 ± 0.03
Hprt1	ACA TTG TGG CCC TCT GTG TG	TTA TGT CCC CCG TTG ACT GA	162	0.99 ± 0.01
36B4	CTT CAT TGT GGG AGC AGA CA	TTC TCC AGA GCT GGG TTG TT	150	0.99 ± 0.01

The primers were designed using Beacon Design 2.0 (Premier Biosoft International, Palo Alto, CA). NT, not tested.

Table 2. Electrophysiological characteristics of primary TAL cells from mouse kidney.

Segment	**V (mV)**	**R (Ohm.cm^2)**	**Ref.**
Mouse PTC	-0.8 ± 0.1	54 ± 1	Terryn et al. 2009
Rabbit mTAL	+ 6-8	212	Jans et al. 2000
Mouse mTAL	-	75-258	Wu et al. 1991
Mouse mTAL	*+ 9.4 ± 0.8*	*73 ± 12*	*This study*

PTC, proximal tubule cells (grey box); mTAL, medullary thick ascending limb (open boxes)

LEGENDS TO FIGURE

Figure 1. Morphological selection of tubule segments.

A. Representative phase contrast images of segments obtained after collagenase treatment of mouse kidneys: proximal convoluted tubules (PCT); proximal straight tubules (PST); thick ascending limbs (TAL); and collecting ducts (CD). Scale bar, 100 μm. **B-C.** Segment-specific marker genes (glomerulus: podocin; PT: AQP1 and SNAT3; TAL: NKCC2 and UMOD; CD: AQP2) were used to demonstrate the purity for each fraction of collected tubule segments using reverse transcriptase PCR (**B**) and SYBR green quantitative PCR (n=6) (**C**).

Figure 2. Morphological characterizations of primary TAL cells.

A. Phase contrast light microscopy demonstrating the development of TAL primary cultures. At day 0, approximately 50 TAL tubules were placed on a 0.33 cm^2 permeable filter support. Formation of small islands of cells was identified after 5 days. The islands expanded and joined around day 10. The filters were confluent after approximately 12 days. Scale bar, 200 μm.

B. Toluidine blue-stained semi-thin section of confluent primary TAL cells on a permeable filter support (Bl, basolateral side; scale bar, 2 μm).

C-F. Representative images obtained by transmission electron microscopy. A complete and two flanking TAL cells positioned on the filter (**C**; scale bar, 2 μm). Magnified panels illustrate the microvilli and endoplasmic reticulum (**D**), mitochondria (**E**) and apical tight junctions and filopodia (**F**). Scale bar, 1 μm.

Figure 3. Immunolocalization of NKCC2, ROMK and uromodulin in mouse primary TAL cultures.

A. Immunofluorescence staining for NKCC2 and uromodulin (UMOD) in primary TAL cells and native mouse kidney sections. NKCC2 is located within the apical membrane, whereas uromodulin shows both apical and additional staining at the extracellular compartment, where it forms filaments (z-scan). A similar pattern is observed in the TAL monolayers and mouse kidney. Scale bar, 10 μm.

B. Immunofluorescent staining for ROMK in primary TAL cells. ROMK staining is concentrated at the apical membrane of the cells (confocal z-scan). Scale bar, 100 μm.

C. Uromodulin filaments present at the apical membrane of fully differentiated (4 days low serum conditions) primary TAL cells (wild-type kidneys) are evidenced by immunofluorescence microscopy. These filaments are absent in primary TAL cells obtained from uromodulin knockout kidneys (inset). Scale bar, 100 μm.

Figure 4. Uromodulin processing in mouse primary TAL cells.

A. Western blot analysis shows NKCC2 expression in primary TAL cells (prTAL, 1 confluent filter after 4 days in low serum conditions), as compared with a pool of 30 micro-dissected TAL, PT and CD segments and total mouse kidney (15 μg total protein). The PT (AQP1) and CD (AQP2) markers are absent in the TAL cells.

B. Western blot demonstrates consistent NKCC2 and uromodulin expression in three lysates of primary TAL cells (1 filter per lane, 4 days low serum conditions).

C. Uromodulin detection in the apical medium of TAL monolayers grown on filters. Secreted uromodulin appears between 4-8h after the wash-out of apical medium (20 μl are loaded in each lane, with baseline (BL) level corresponding to the last 48h of

culture). Upon longer exposure of the film to the blotting membrane, uromodulin secretion appears already 2 h after washing.

D. Treatment of confluent TAL monolayers with protease inhibitor cocktail (PIC) for 16h (apical side) significantly reduced the cleavage of uromodulin and its release into the apical medium. Representative immunoblots, with 20 µl of apical medium loaded in each lane. Quantification by densitometry reveals that the level of uromodulin secreted is reduced after PIC treatment (35.3 ± 13 % of control value; n=4; p=0.01).

Figure 5. NanoLC–ESI-MS/MS analysis of uromodulin expressed by primary TAL cells.

A. Western blot analysis (anti-uromodulin) of deglycosylated (PNGaseF) purified proteins from primary TAL cell apical medium (prTAL) or urine. The short uromodulin isoform released by primary TAL cells has similar molecular weight as the urinary protein (red arrows). **B.** Coomassie-stained gel showing deglycosylated proteins purified from apical primary TAL cell medium (prTAL) or urine-purified uromodulin. The red arrows indicate the band that was analyzed by MS. **C.** Mouse uromodulin protein sequence (Uniprot accession Q91X17). MS sequence coverage of uromodulin from primary TAL apical medium is shown (62% over the entire protein). The C-terminal most abundant peptide identified by MS analysis is shown in bold underlined. This peptide ends at F588, the same C-terminal residue reported for murine urinary uromodulin [38]. **D.** MS profile of differently charged (z2+, z3+ or z4+) C-terminal peptides from uromodulin released in primary TAL cell apical medium. The large majority of peptides ends at residue F588. **E.** Representative MS/MS spectra confirming the identity of C-terminal peptides ^{573}DSTSEQCKPTCSGTRF^{588} and ^{573}DSTSEQCKPTCSGTRFR^{589}.

Figure 6. Functional characterization of primary TAL cells.

A. A lumen-positive transepithelial voltage (V_{te}) averaging 11.5±1.4 mV is observed at baseline (Bl) across primary TAL monolayers. V_{te} is reduced to 2.2±0.6 mV upon treatment with 100 μM bumetanide (Bum; n=7; p=0.001), with recovery 20 min after wash-out.

B. V_{te} is significantly reduced in TAL monolayers obtained from ROMK knockout (ko) vs. wild-type (ctrl) mice (n=6; p<0.001). Inset: reverse transcriptase-PCR analysis showing lack of ROMK mRNA expression in TAL cells from ROMK knockout mice.

C. The vasopressin type-2 receptor (AVPR2) is expressed in primary TAL cells (inset). Treatment of TAL monolayers with DDAVP (5min) yields a dose-dependent increase in intracellular cAMP concentration (n=4 for each concentration).

D. The effect of DDAVP is markedly larger when applied on the basolateral side of the primary TAL monolayers (cAMP levels after 5 min apical vs. basolateral exposure to 10 nM DDAVP; n=6; p<0.01).

E. Quantitative PCR analyses show a typical response to hypoxia, with increased pyruvate dehydrogenase 2 (PHD2; 5.16±0.96 vs. 1.00±0.16; n=4; p=0.03) and glucose transporter (GLUT1; 2.32±0.29 vs. 1.00±0.17; n=4; p<0.01) mRNA expression levels) contrasting with stable PHD1 in primary TAL cells exposed for 24 h to 0.2% vs. 21% oxygen (control).

F. Quantitative PCR analyses demonstrate increased tonicity-responsive enhancer-binding protein (TonEBP; 2.16±0.31 vs. 1.00±0.07; n=4; p=0.03), heat shock protein 70 (HSP70; 7.96±0.65 vs. 1.00±0.05 ; n=4; p=0.002) and aldose reductase (AR; 25.96±3.20 vs. 1.00±0.05; n=4; p=0.004) upon exposure of the primary TAL monolayers for 6 h to hypertonic (480 mOsm) vs. control (320 mOsm) medium.

Figure 7. Transfectability of primary TAL cells.

A. Lipofectamin-mediated transfection of BLOCK-iT^{TM} Alexa555 Red siRNA in primary TAL cells, showing fluorescent staining (i.e. internalization of the Alexa555 siRNA) in a large proportion of cells. Control primary TAL cells were transfected with a non-fluorescent Silencer^{R}Negative control siRNA. Scale bar, 50 μm.

B. Specific siRNA targeting of endogenous uromodulin (UMOD) mRNA expression in primary TAL cells. Primary TAL cells transfected with UMOD targeting siRNAs show a significant reduction in *Umod* (100 ± 2% vs. 49 ± 7%, respectively; $p<0.001$; n=6), whereas the expression of the non-specific target *Clcn5* is not affected (100 ± 8% vs. 91 ± 8%, respectively; n=6). Control primary TAL cells were similarly transfected with a Silencer^{R}Negative control siRNA.

Figure 1

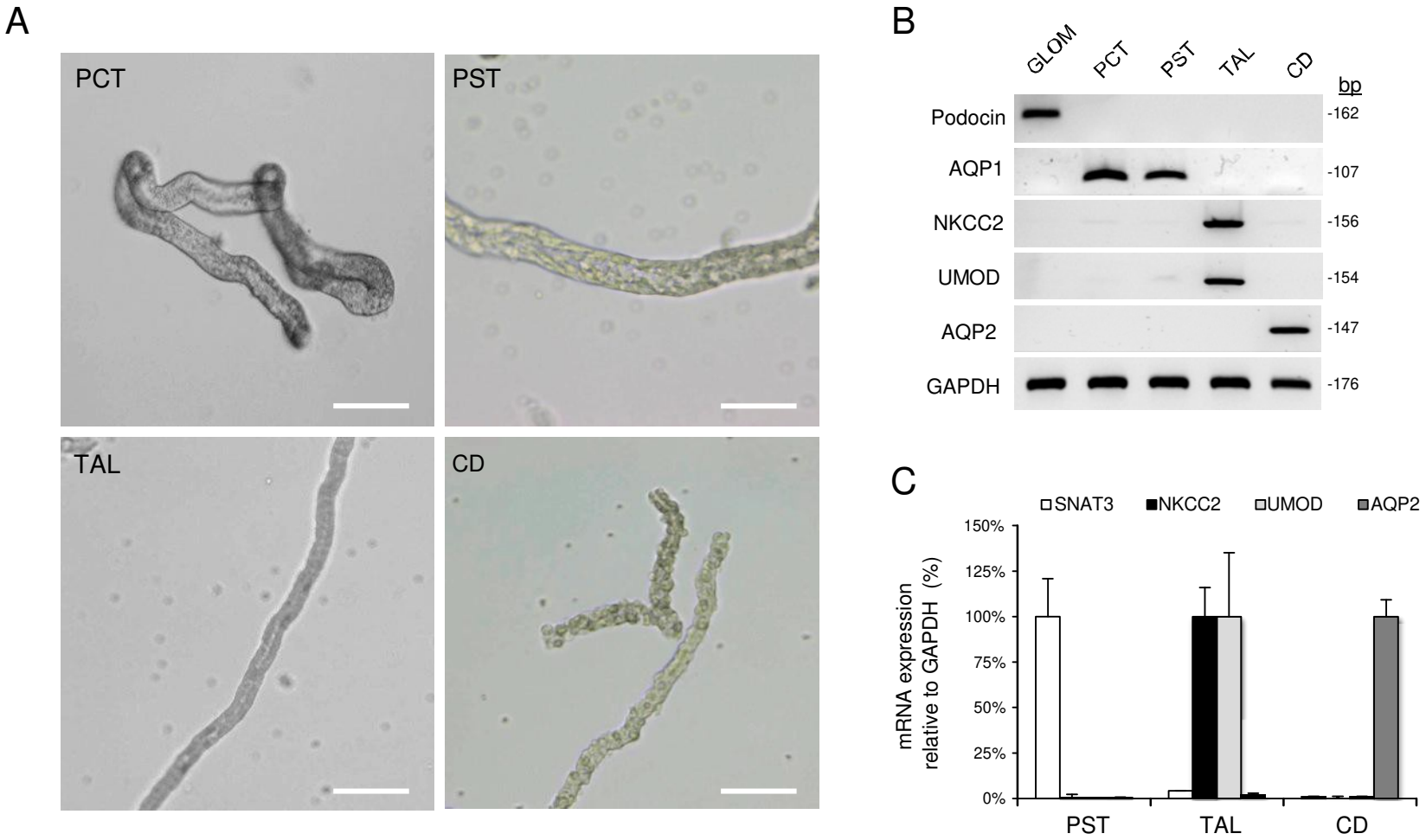
A
PCT
PST
TAL
CD
B
GLOM
PCT
PST
TAL
CD
bp
Podocin
-162
AQP1
-107
NKCC2
-156
UMOD
-154
AQP2
-147
GAPDH
-176
C
SNAT3
NKCC2
UMOD
AQP2
mRNA expression relative to GAPDH (%)
150%
125%
100%
75%
50%
25%
0%
PST
TAL
CD

Figure 2

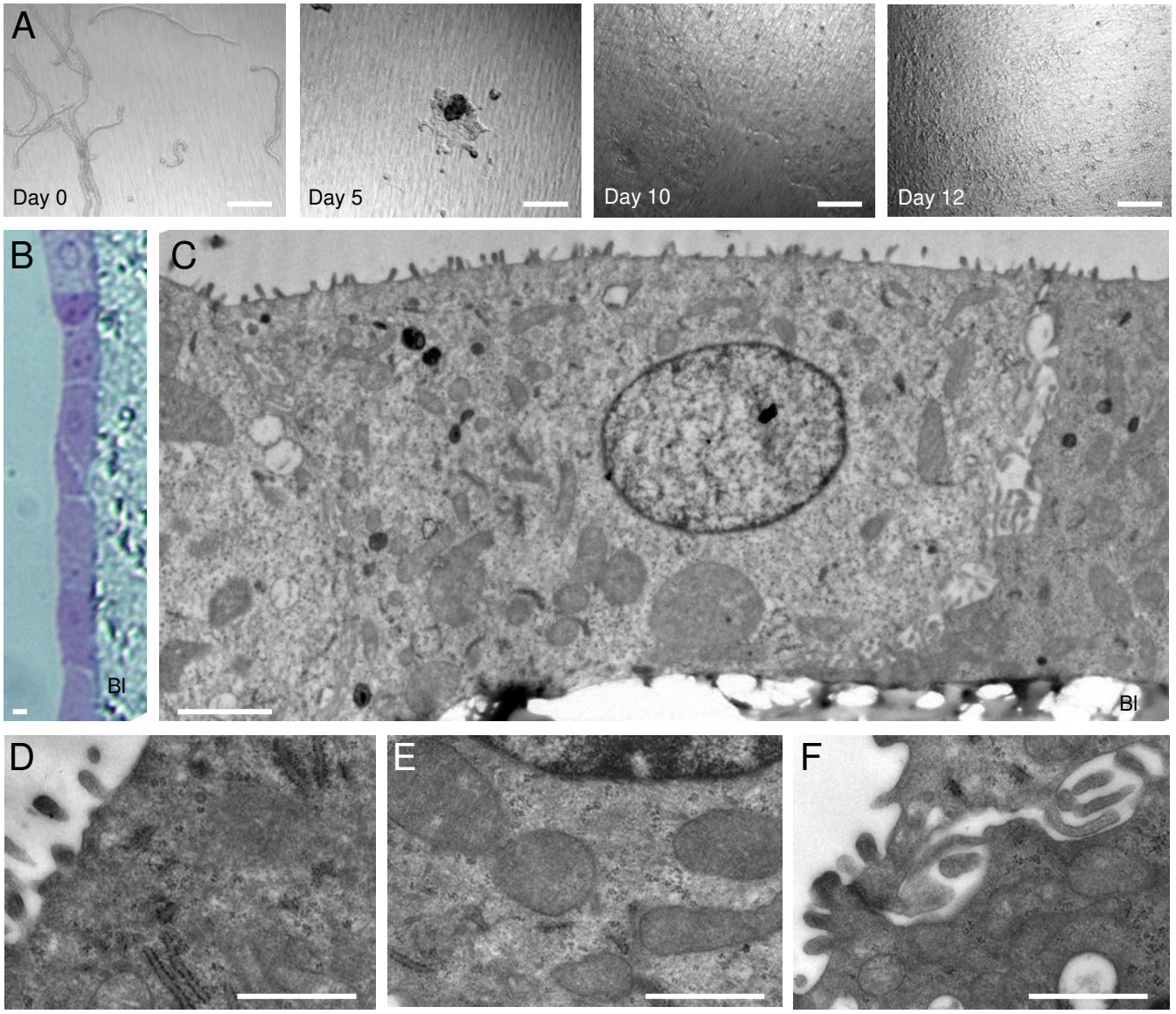

Figure 3

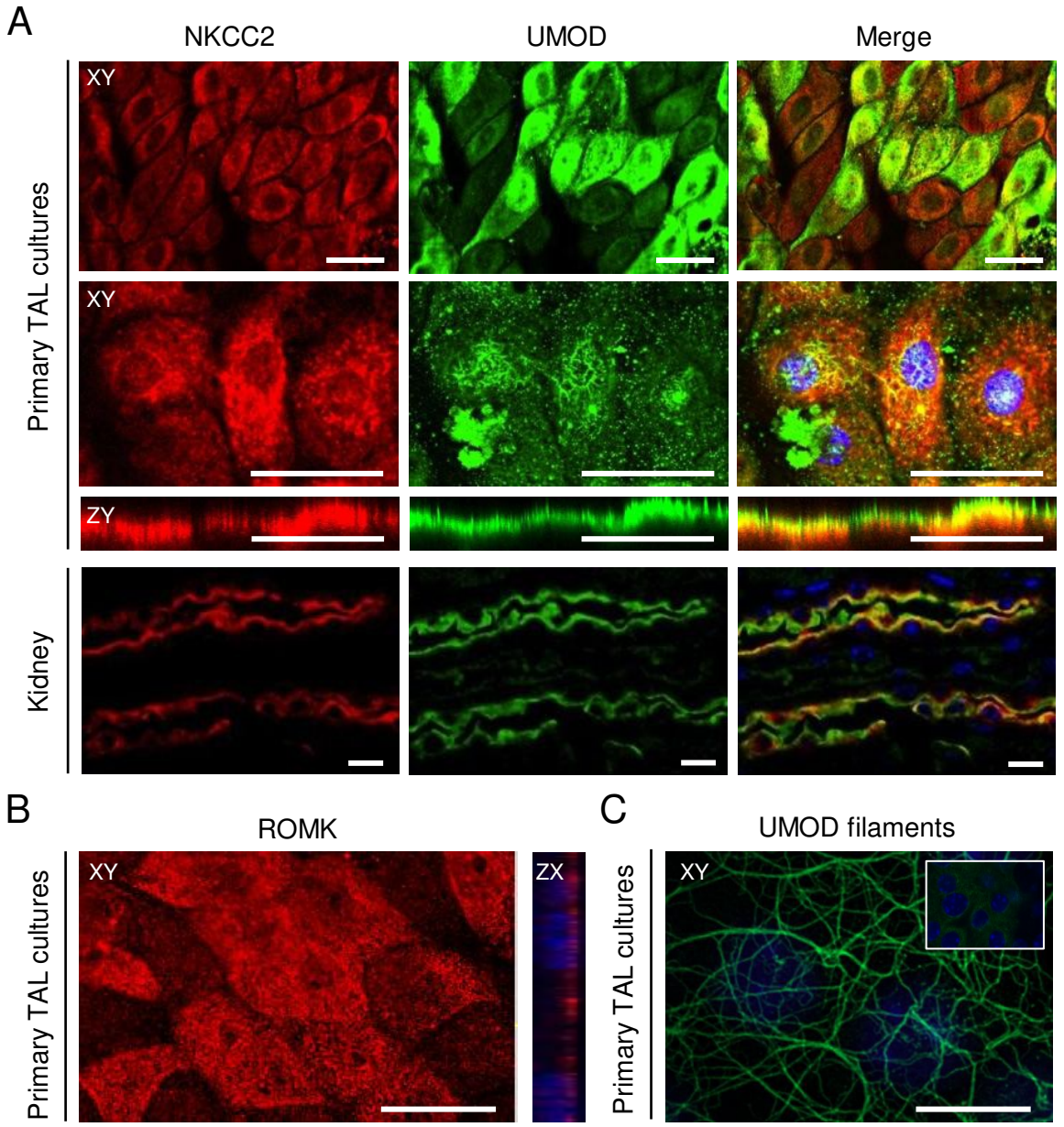
A
NKCC2
UMOD
Merge
XY
XY
ZY
Primary TAL cultures
Kidney
B
ROMK
XY
ZX
Primary TAL cultures
C
UMOD filaments
XY
Primary TAL cultures

Figure 4

A

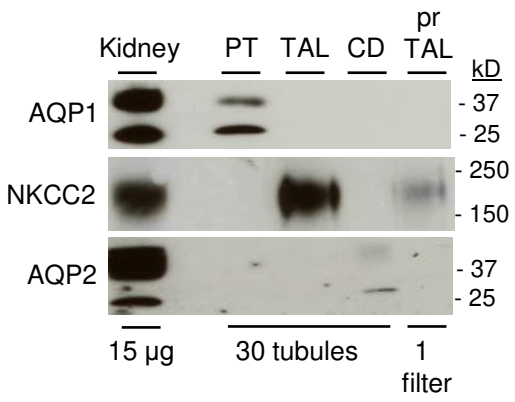

B

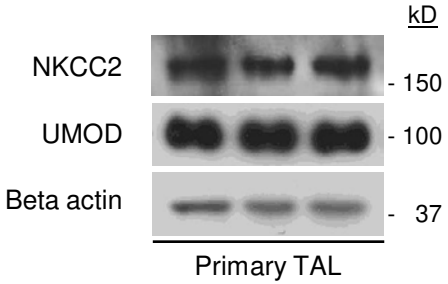

C

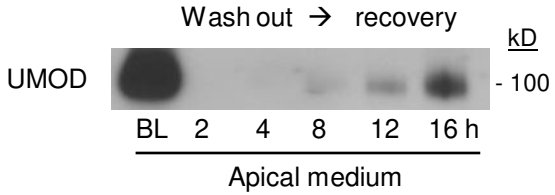

D

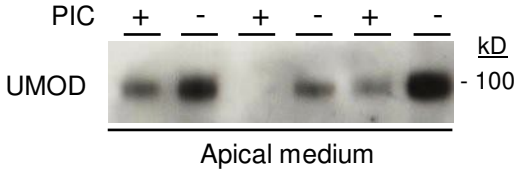

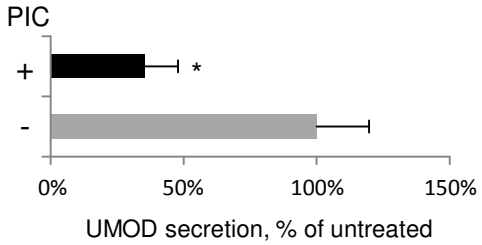

Figure 5

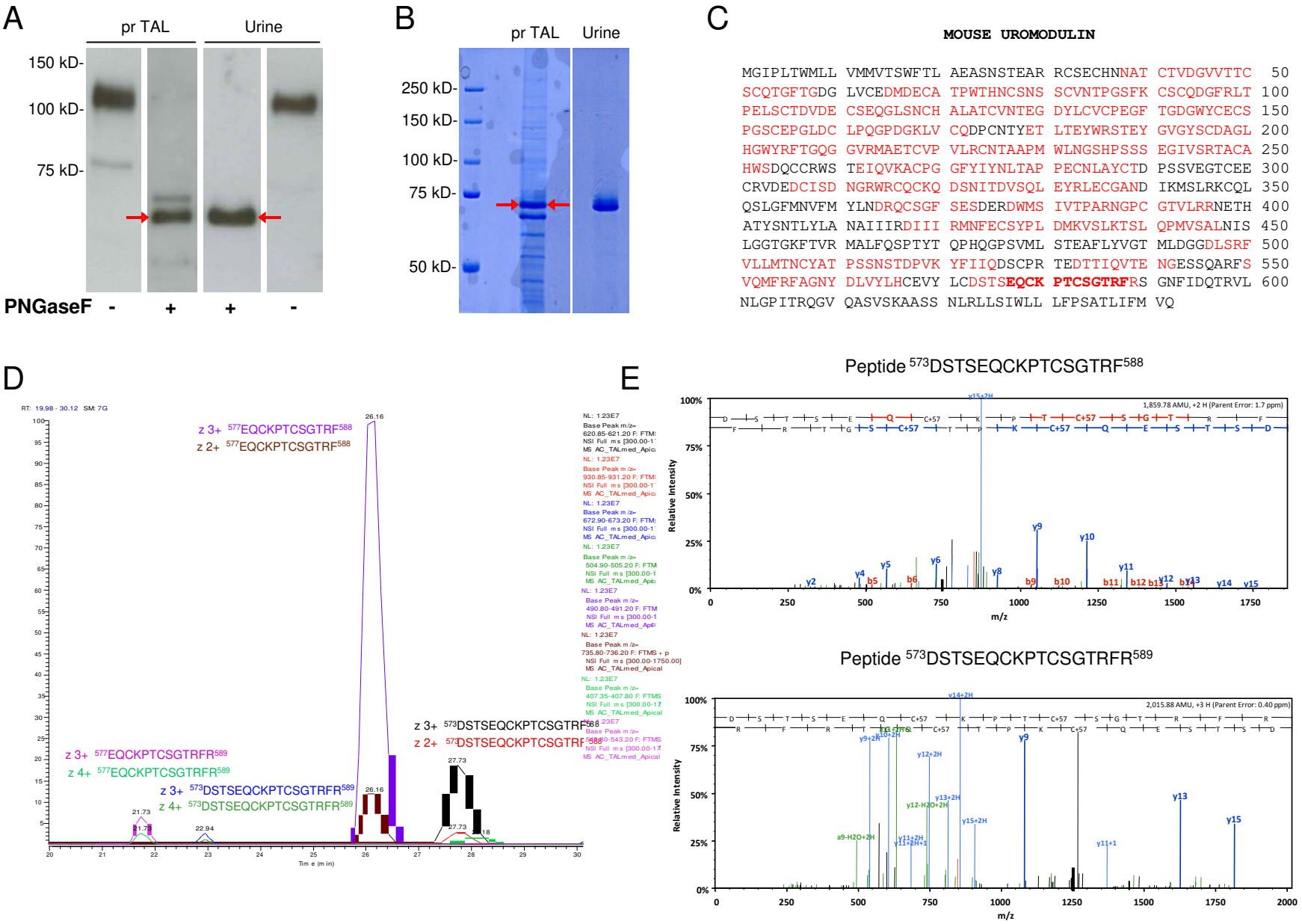
A
pr TAL
Urine
150 kD-
100 kD-
75 kD-
PNGaseF - + + -
B
pr TAL
Urine
250 kD-
150 kD-
100 kD-
75 kD-
50 kD-
C
MOUSE UROMODULIN
MGIPLTWMLL VMMVTSWFTL AEASNSTEAR RCSECHNNAT CTVDGVVTTC 50
SCQTGFTGDG LVCEDMDECA TPWTHNCSNS SCVNTPGSFK CSCQDGFRLT 100
PELSCTDVDE CSEQGLSNCH ALATCVNTEG DYLCVCPEGF TGDGWYCECS 150
PGSCEPGLDC LPQGPDGKLV CQDPCNTYET LTEYWRSTEY GVGYSCDAGL 200
HGWYRFTGQG GVRMAETCVP VLRCNTAAPM WLNGSHPSSS EGIVSRTACA 250
HWSDQCCRWS TEIQVKACPG GFYIYNLTAP PECNLAYCTD PSSVEGTCEE 300
CRVDEDCISD NGRWRCQCKQ DSNITDVSQL EYRLECGAND IKMSLRKCQL 350
QSLGFMNVFM YLNDRQCSGF SESDERDWMS IVTPARNGPC GTVLRRNETH 400
ATYSNTLYLA NAIIIRDIII RMNFECSYPL DMKVSLKTSL QPMVSALNIS 450
LGGTGKFTVR MALFQSPTYT QPHQGPSVML STEAFLYVGT MLDGGDLSRF 500
VLLMTNCYAT PSSNSTDPVK YFIIQDSCPR TEDTTIQVTE NGESSQARFS 550
VQMFRFAGNY DLVYLHCEVY LCDSTSEQCK PTCSGTRFRS GNFIDQTRVL 600
NLGPITRQGV QASVSKAASS NLRLLSIWLL LFPSATLIFM VQ
D
RT: 19.98 - 30.12 SM: 7G
z 3+ 577EQCKPTCSGTRF588
z 2+ 577EQCKPTCSGTRF588
z 3+ 577EQCKPTCSGTRFR589
z 4+ 577EQCKPTCSGTRFR589
z 3+ 573DSTSEQCKPTCSGTRFR589
z 4+ 573DSTSEQCKPTCSGTRFR589
z 3+ 573DSTSEQCKPTCSGTRF588
z 2+ 573DSTSEQCKPTCSGTRF588
Time (min)
E
Peptide 573DSTSEQCKPTCSGTRF588
1,859.78 AMU, +2 H (Parent Error: 1.7 ppm)
Relative Intensity
m/z
Peptide 573DSTSEQCKPTCSGTRFR589
2,015.88 AMU, +3 H (Parent Error: 0.40 ppm)
Relative Intensity
m/z

Figure 6

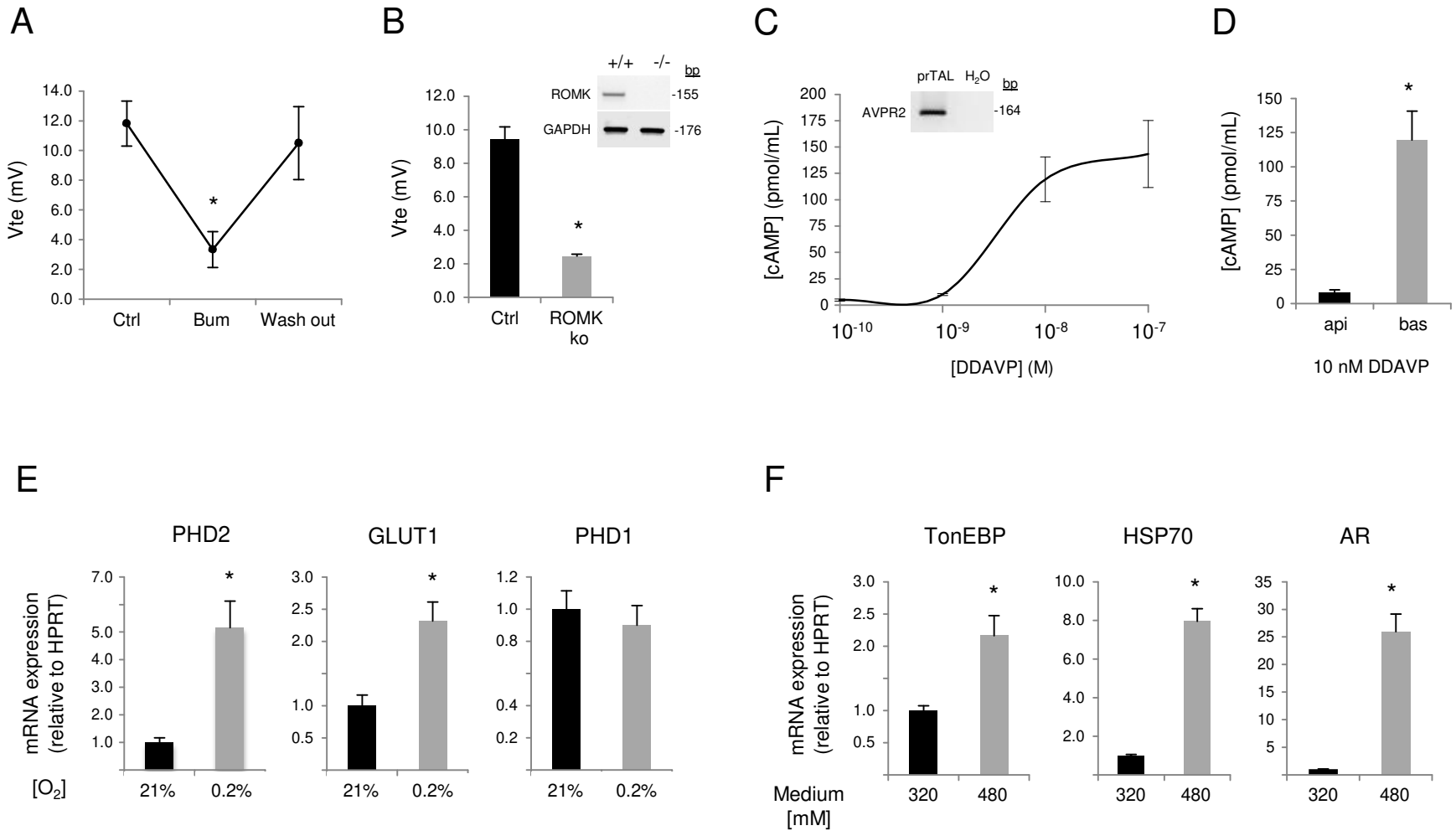
A
Vte (mV)
14.0
12.0
10.0
8.0
6.0
4.0
2.0
0.0
*
Ctrl
Bum
Wash out
B
Vte (mV)
12.0
10.0
8.0
6.0
4.0
2.0
0.0
+/+
-/-
bp
ROMK
-155
GAPDH
-176
*
Ctrl
ROMK ko
C
[cAMP] (pmol/mL)
200
175
150
125
100
75
50
25
0
prTAL
H2O
bp
AVPR2
-164
10-10
10-9
10-8
10-7
[DDAVP] (M)
D
[cAMP] (pmol/mL)
150
125
100
75
50
25
0
*
api
bas
10 nM DDAVP
E
PHD2
GLUT1
PHD1
mRNA expression (relative to HPRT)
7.0
5.0
4.0
3.0
2.0
1.0
3.0
2.5
2.0
1.0
0.5
1.2
1.0
0.8
0.4
0.2
*
*
[O2]
21%
0.2%
21%
0.2%
21%
0.2%
F
TonEBP
HSP70
AR
mRNA expression (relative to HPRT)
3.0
2.5
2.0
1.0
0.5
10.0
8.0
6.0
4.0
2.0
35
30
25
20
15
10
5
*
*
*
Medium [mM]
320
480
320
480
320
480

Figure 7

A

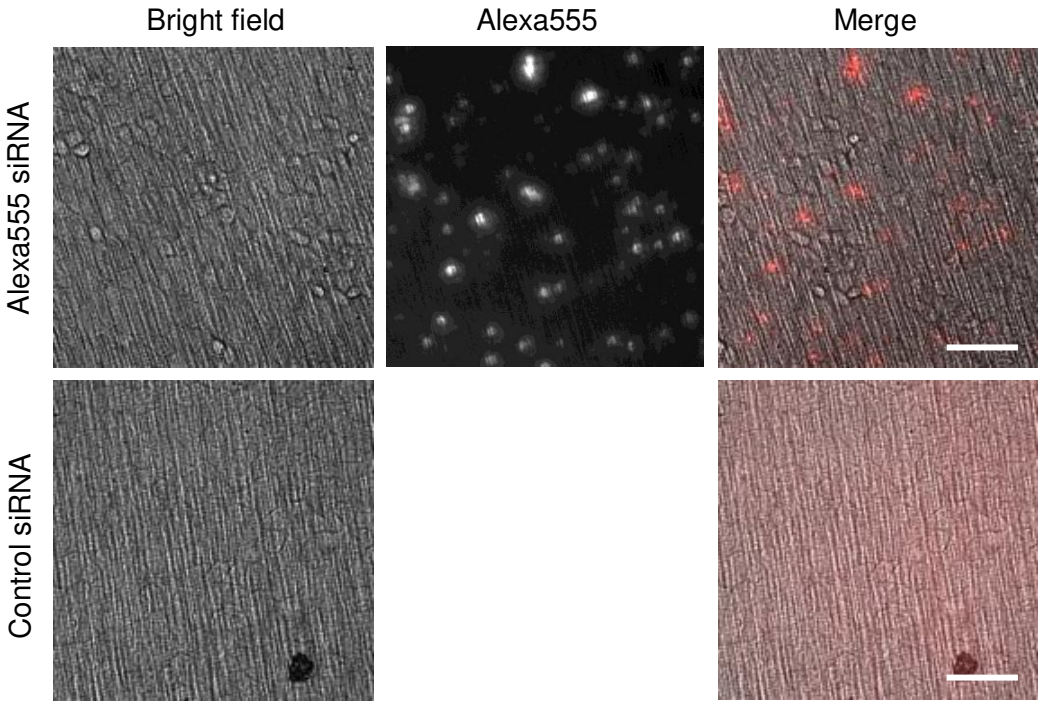
Bright field
Alexa555
Merge
Alexa555 siRNA
Control siRNA

B

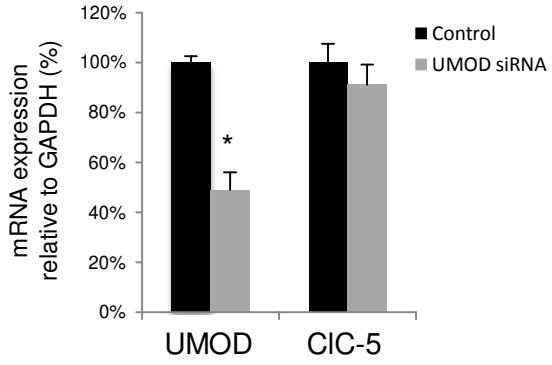
120%
100%
80%
60%
40%
20%
0%
mRNA expression relative to GAPDH (%)
Control
UMOD siRNA
*
UMOD
ClC-5